



**HAL**  
open science

# Theoretical study of the insertion and diffusivity of hydrogen in the Ti<sub>3</sub>Al-D0<sub>19</sub> system: comparison with Ti-hcp and TiAl-L1<sub>0</sub> systems

Damien Connetable

► **To cite this version:**

Damien Connetable. Theoretical study of the insertion and diffusivity of hydrogen in the Ti<sub>3</sub>Al-D0<sub>19</sub> system: comparison with Ti-hcp and TiAl-L1<sub>0</sub> systems. *International Journal of Hydrogen Energy*, 2019, 44 (60), pp.32307-32322. 10.1016/j.ijhydene.2019.10.095 . hal-02347017

**HAL Id: hal-02347017**

**<https://hal.science/hal-02347017>**

Submitted on 5 Nov 2019

**HAL** is a multi-disciplinary open access archive for the deposit and dissemination of scientific research documents, whether they are published or not. The documents may come from teaching and research institutions in France or abroad, or from public or private research centers.

L'archive ouverte pluridisciplinaire **HAL**, est destinée au dépôt et à la diffusion de documents scientifiques de niveau recherche, publiés ou non, émanant des établissements d'enseignement et de recherche français ou étrangers, des laboratoires publics ou privés.

# Theoretical study of the insertion and diffusivity of hydrogen in the $\text{Ti}_3\text{Al-}D0_{19}$ system: comparison with Ti-hcp and TiAl- $L1_0$ systems.

Damien Connétable<sup>a,\*</sup>

<sup>a</sup>CIRIMAT, UMR 5085, CNRS INP UPS, ENSIACET 4, allée Émile Monso, BP 44362, F-31030 Toulouse Cedex 4, France

---

## Abstract

Using first-principles calculations, the insertion and diffusivity of hydrogen in the  $\text{Ti}_3\text{Al-}D0_{19}$  system are presented and discussed. After a brief description of the properties of  $\text{Ti}_3\text{Al}$ , the different sites of insertion are identified and discussed. The octahedral configuration surrounded by Ti atoms only ( $2a$  Wyckoff position) is found to be the preferred insertion site for H atoms. The second octahedral and the two tetrahedral sites are found significantly less stable than  $2a$  sites. Phonon, electronic and elastic properties were computed to analyze the interactions between hydrogen and the metal. Results show that hydrogen atoms interact little with the metal. The insertion into a  $2a$  site minimizes the elastic deformation and electronic transfer of surrounding atoms. The diffusion coefficient of hydrogen is then calculated and discussed by using DFT simulations, kinetic Monte-Carlo simulations and a multi-site approach. These results are compared with those of H diffusion into the Ti-hcp and TiAl- $L1_0$  systems.

**Keywords:**  $\text{Ti}_3\text{Al}$ , hydrogen, DFT, solubility, diffusivity, intermetallic

---

## 1. Introduction

The renewed interest in Ti-Al alloys leads us to study the mechanisms of embrittlement by hydrogen or by other interstitial species. More precisely, the role of H is known to induce a premature failure of metallic systems, known as hydrogen embrittlement (HE). Various interpretations of the process and theory are used to explain how hydrogen weakens metals. The two main prevailing HE concepts are *Hydrogen Enhanced Localized Plasticity* (HELP) [1] and *Hydrogen Enhanced Decohesion* (HEDE) [2]. These models were developed to explain the physical origin of H induced fracture. They take into account the segregation of H at dislocations, interfaces, interphases and the formation of cluster-type defects. These mechanisms are still widely debated and under study. Their better understanding requires deeper knowledge of basic properties, such as the amount of hydrogen dissolved in the metal, of its diffusion coefficients and hydrogen-metal interactions. Atomistic simulations can play a crucial role in providing insight into the plasticity and fracture.

The aim of this work is thus to improve the understanding of the behavior of interstitial species during their use and ageing. The use of innovative manufacturing processes, such as additive machines and SPS techniques, have made it possible to use and shape TiAl materials. The presence of different sub-structures, in the form of precipitates or phases, is sought to obtain the desired mechanical properties. In TiAl systems, apart from the  $\gamma$ -TiAl- $L1_0$  phase which is the main stable phase, the other phases

are precipitates like the lamellar  $\alpha_2$ - $\text{Ti}_3\text{Al-}D0_{19}$ . This titanium-rich phase is chemically close to the  $\alpha$ -Ti-hcp structure.  $\text{Ti}_3\text{Al}$  can also happen during the high temperature oxidation process that occurs on the surface by depleting Al atoms from under the surface. The growth of the oxide causes a change in chemistry resulting locally in a phase change:  $\gamma$ -TiAl becomes  $\alpha_2$ - $\text{Ti}_3\text{Al}$ , which in turn may become titanium. Therefore, as a means to better understand the general behavior of hydrogen in titanium-based alloys, it is important to explain and predict its behavior not only in TiAl, as has been done in the past, but also in the  $D0_{19}$  system. Even though this phase is a minority phase, it is no less important in order to better understand the solubility and diffusivity of hydrogen.

Literature results show that hydrogen dissolves easily in titanium-rich phases, and particularly in Ti-hcp [3–7], for which hydrogen atoms have an insertion energy of -0.44 eV into titanium octahedral sites. In a recent study on the insertion of H in TiAl, Connétable [8] showed that H was preferentially positioned in sites rich in Ti atoms. Hydrogen is therefore expected to dissolve more easily in  $\text{Ti}_3\text{Al}$  than in TiAl [3, 4]. It is important to determine whether this difference is significant and how hydrogen diffuses, so as to compare results with other Ti systems. Experimentally, Miyoshi [9] and Naito [10, 11] showed that H atoms diffuse slower in  $\alpha_2$  than in other TiAl phases.

This work thus focuses thoroughly on the processes of insertion and diffusivity of H atoms. The interactions between other defects, i.e. interphases, grain-boundaries [12], vacancies (like super-abundant vacancies [13]) and surfaces were neglected here and assumed negligible in first-approximation. This work falls into the framework of the study of hydrogen in the limit of infinite dilution. Moreover, before focusing on the weakening of interfaces, a reliable database on the energies and in-

---

\*Corresponding author

Email address: damien.connetable@ensiacet.fr (Damien Connétable)

sorption sites of H in the  $DO_{19}$  system must be obtained. It is indeed a prerequisite before introducing degree of complexity, and this work fits well into the general framework of the study of H embrittlement in TiAl systems.

After having conducted a complete study of the hydrogen insertion and diffusivity in the TiAl- $L1_0$  system [8], the case of H atoms in the  $Ti_3Al-DO_{19}$  system is discussed hereinafter. While the TiAl- $L1_0$  study focused on insertion sites, here, an exhaustive study of the insertion in the  $DO_{19}$  system is performed. Insertion sites are clearly identified and additional information is given to characterize the insertion of H atoms at different scales (volume of relaxation, elastic dipoles, etc.). The diffusion mechanisms are then studied in detail. The use of kinetic Monte Carlo simulations and a multi-site approach [14, 15] are the appropriate tools to study anisotropic properties. Hydrogen diffusion coefficients will then be discussed and compared with those in the TiAl- $L1_0$  system, but also to those in the Ti-hcp system, for which the diffusion coefficient formulas were also developed. Subsequently, results will thus be used specifically for this  $Ti_3Al$  system, but also in the case of other  $DO_{19}$  systems.

Section 2 presents the method and calculation details. In section 3, the ground-state properties of the  $Ti_3Al$  system are briefly described and compared with experimental and theoretical literature, as well as with other TiAl systems. The insertion of H atoms in the  $Ti_3Al$  system is investigated in section 4. The diffusion mechanisms are subsequently discussed in section 5, and, to conclude, hydrogen diffusivity is presented.

## 2. Methodology

First-principles calculations were computed using the VASP code [16]. The plane-wave basis projector augmented wave method (PAW) [17, 18] and the Perdew-Burke-Ernzerhof generalized gradient approximation of the exchange and correlation functional (PBE [19]) were employed in the framework of the DFT. Like all other TiAl systems [5, 8, 20], the  $Ti_3Al$  system is not magnetic. Calculations were thus performed without magnetism. For the  $H_2$  molecule, however, the DFT energy was computed with spin effects. The plane-wave energy cut-off was set to 600 eV, and  $20 \times 20 \times 20$   $\Gamma$ -centered Monkhorst-Pack meshes [21] were used to sample the first Brillouin zone of the primitive cell (8 atoms). For super-cells, the band-folding method was used. Forces between ions were relaxed. Calculations were performed at zero pressure (relaxed volume and shapes of super-cells), except for the computation of elastic dipoles.

The study of migration processes was conducted through NEB simulations [22] on  $2 \times 2 \times 2$  super-cells (i.e. 64 atoms per super-cell). Transition state energies were computed with the same accuracy as stable position energies. The vibrations for the stable and transition states were computed to quantify jump rates,  $\Gamma_{xy}$ , and to study the stability of the configurations. The *phonopy* package [23] was then used to compute inter-atomic force constants (IFC), phonon free energies and to analyze band structures.

## 3. Ground state properties of the $Ti_3Al-DO_{19}$ structure

$Ti_3Al-DO_{19}$  has a hexagonal closed-packed structure belonging to space-group 194 ( $hP8$ ,  $P6_3/mmc$ ). Ti atoms occupy the  $6h$  sites ( $x_h$ ,  $2x_h$ ,  $1/4$ ) and Al atoms the  $2c$  sites ( $1/3$ ,  $2/3$ ,  $1/4$ ) [24], as displayed in Fig. 1.

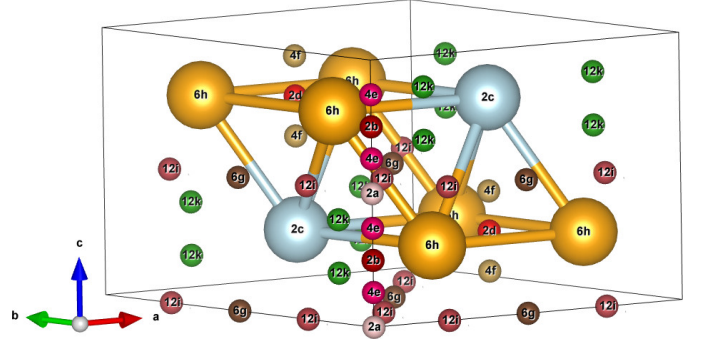


Figure 1: Schematic representation of the  $Ti_3Al$  structure: Ti and Al atoms are in yellow and blue, respectively. H insertion sites that were tested are also represented.

DFT values of the ground state of the  $Ti_3Al$  system, lattice parameters ( $a_0$  and  $c_0$ ) and formation energy ( $E_f$ ), are summarized in Table 1. The formation energy (in eV per atom) corresponds to:

$$E_f[Ti_nAl_m] = \frac{E_o[Ti_nAl_m] - nE_o[Ti-hcp]/2 - mE_o[Al-fcc]}{n + m} \quad (1)$$

where  $E_o[Y]$  are the DFT energies of the  $Y$  system.

Results on the  $Ti_3Al$  system are compared with earlier theoretical and experimental literature, as well as with other stable TiAl binaries, namely: TiAl- $L1_0$  (space group 123, with Ti and Al atoms in  $1a$  and  $1d$  sites, respectively see Ref. [8]), TiAl- $B2$  (space group 221, with Ti and Al atoms in  $1a$  and  $1b$  sites, respectively),  $TiAl_2$  (space group 141,  $tI24$ , with Ti and Al atoms in  $8e$  sites),  $TiAl_3-DO_{22}$  (space group 139, with Ti in  $2a$  sites, and Al  $2b$  and  $4d$  sites), and reference states (hcp-Ti and fcc-Al). Values are given in Table 1. Experimental data were extracted from Schuster and Palm's reassessment [25] of the Ti-Al phase diagram.

The first focus is on the properties of  $Ti_3Al$ . The relaxed Ti position in the  $DO_{19}$  system,  $x_h$ , is found equal to 0.830, in excellent agreement with the experimental value  $x_h \approx 0.833$  [39]. DFT values of lattice parameters (5.75 and 4.65 Å) are also found in excellent agreement with experimental data (5.77 and 4.65 Å) [32, 33, 39]. The difference between PBE and experimental values is smaller than 0.7%. The DFT formation energies, about -280 meV, also agree well with experimental values, in the range of [-309; -218] meV [25]. These results show that DFT simulations match experimental observations and can be considered reliable.

As regards ground states properties of the  $Ti_3Al$  system (elastic constants, electronic density-of-states and band structure, not shown here for simplification purposes), the present simulations reproduced exactly the results of Bakulin *et al.* [40] and

Table 1: Theoretical and experimental lattice parameters  $a_o$  and  $c_o$  (in Å), formation energies ( $E_f$ , in meV/atom), bulk ( $B$ , in GPa) and Young ( $E$ , in GPa) modulus, elastic constants ( $C_{ij}$ , in GPa) and Poisson coefficient ( $\nu$ ).

		$a_o$	$c_o$	$E_f$	$B$	$E$	$\nu$
Ti (hcp)	PBE [8]	2.938	4.657	0	112	123	0.32
	exp. [26]	2.945	4.544	-	112	-	-
Ti <sub>3</sub> Al ( <i>D0</i> <sub>19</sub> )	this work	5.752	4.656	-282	115	152	0.28
	PW91 [27]	5.72	4.633	-	-	-	-
	PBE [28]	5.734	4.640	-	-	-	-
	exp.	5.77/5.792 [29, 30]	4.645 [29, 30]	-309/-218 [25]	114 [31]	151 [31]	-
TiAl ( <i>L1</i> <sub>0</sub> )	PBE [8]	3.999	4.076	-407	114	171	0.25
	exp.	3.97/4.01 [32, 33]	4.04/4.08 [32, 33]	-392 [32]	110 [34]	183 [34]	-
TiAl ( <i>B2</i> )	this work	3.186	-	-266	-	-	-
TiAl <sub>3</sub> ( <i>D0</i> <sub>22</sub> )	this work	3.844	8.624	-398	106	208	0.17
	PBE [35]	3.847	8.621	-396	-	-	-
	exp.	3.84/3.848 [29, 36]	8.579/8.596 [29, 36]	-383 [25]	-	-	-
Al (fcc)	PBE [8]	4.04	-	0	78	72	0.35
	exp. [26]	4.05	-	-	78	-	-
		$C_{11}$	$C_{33}$	$C_{44}$	$C_{66}$	$C_{12}$	$C_{23}$
Ti (hcp)	PBE [8]	176	188	43	47	82	76
	exp. [37]	172	180	44	45	82	76
Ti <sub>3</sub> Al ( <i>D0</i> <sub>19</sub> )	this work	189	232	51	59	87	64
	PW91 [27]	185	231	57	51	83	63
	exp. [33, 38]	175	219	63	-	88	62
TiAl ( <i>L1</i> <sub>0</sub> )	PBE [8]	171	172	112	64	88	85
	exp. [34]	186	176	101	77	72	74
	[33]	187	182	109	81	75	75
TiAl ( <i>B2</i> )	this work	82	-	70	-	127*	-
TiAl <sub>3</sub> ( <i>D0</i> <sub>22</sub> )	this work	193	218	94	129	86	45
	PBE [35]	190	213	96	127	87	46
	exp. [36]	218	218	92	116	58	45
Al (fcc)	PBE [8]	105	-	33	-	65	-
	exp. [26]	106	-	31	-	65	-

Zeng [41]. These works used the same approach, i.e. the DFT-PBE-PAW method. However, results are complemented here with the phonon properties. The inter-atomic force constants (IFCs) were calculated on the primitive cell (i.e. 8 atoms). The plots of the phonon band structure and phonon projected density-of-states (calculated on  $30 \times 30 \times 30$   $\mathbf{q}$ -meshes grids) are displayed in Fig. 2. The analysis of the phonon density-of-states projected onto Ti and Al species clearly shows that acoustic dispersion curves are almost entirely associated with Ti atoms. This result is consistent with the mass ratio between Al and Ti atoms and the stoichiometry (1:3). As for the optic modes, they are associated with Al atoms. The small gap in the phonon spectra is specific of this structure as compared with other Ti-Al alloys (see for example TiAl-*L1*<sub>0</sub>, Ref. [8]). The dispersion curves around  $\mathbf{q}=\Gamma$ , associated with the sound velocity, do not show any anomaly, in agreement with elastic properties and stability criteria, see Mouhat [42]. From these phonon properties, the heat capacity,  $C_v$ , (plotted in Appendix A) and the phonon free energy were computed, thereafter used to determine the zero-point energy of H atom inserted in the metal.

The comparison with other binary systems is henceforth possible. Among all TiAl systems studied, results show that

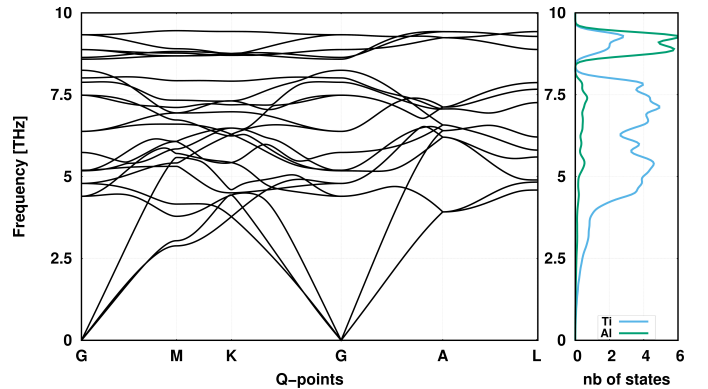


Figure 2: Phonon band structure (*pBAND*) and projected density-of-states (*pDOS*) of Ti<sub>3</sub>Al-*D0*<sub>19</sub> primitive cell. The blue and orange lines correspond to the projected DOS of the Ti and Al atoms, respectively. Frequencies are expressed in THz.

the TiAl-*L1*<sub>0</sub> structure has the lowest formation energy. In all cases studied here, DFT PBE simulations reproduce the ground states properties of stable TiAl systems with an excellent accuracy. For instance, the elastic constants computed using finite

displacements method as implemented in VASP (on primitive cells) are excellent. These results can be used as reference parameters. One system however shows irregularities: the TiAl-B2 system. At 0K, it is an unstable phase. Indeed,  $C_{12}$  of the TiAl-B2 system (equal to 127GPa) is found greater than  $C_{11}$  (82GPa). One of Born's three stability criteria [42] (for cubic systems) is thus not verified,  $C' = (C_{11} - C_{12})/2$  is negative. This result is in agreement with experimental findings, which indicate that the TiAl-B2 system is unstable at low temperature [39].

To conclude, data provided by DFT simulations accurately reproduce bulk properties, H insertion can now be studied.

#### 4. Hydrogen solubility

To study the hydrogen insertion, a quick analysis of interstitial sites inside the  $\text{Ti}_3\text{Al-DO}_{19}$  system is necessary. Part of the work conducted by Bakulin *et al.* [40], in their study on oxygen insertion, can be used here. They identified four insertion sites, labeled O1, O2, T1 and T2. The O1 site is formed of six Ti atoms while O2 is at the center of the octahedron formed of four Ti atoms and two Al atoms. T1 and T2 are tetrahedrons formed of three Ti atoms and one Al atom. Nevertheless, a complete analysis of the  $\text{DO}_{19}$  system reveals there are many possible interstitial sites [24]:  $2a, 2b, 2d, 4e, 4f, 6g, 6h, 12i, 12j$  and  $12k$  sites. The atomic positions are summarized in Table 2 and represented in Fig. 1. The tetrahedral (resp. octahedral) sites correspond therefore to the  $12k$  and  $4f$  (resp.  $2a$  and  $6g$ ) sites. A correlation can now be made between the notations of Bakulin [40] and crystallographic notations:  $O1 = 2a, O2 = 6g$  and  $12k = T1, 4f = T2$ . The other sites are located on the faces or the edges of the octahedron or tetrahedron volumes. These sites have already been identified as potential insertion sites for fcc and hcp phases [43–45], this is why they were considered.

To evaluate the relative stability of configurations, hydrogen insertion energies,  $E_i$ , were computed. Calculations were conducted on  $2 \times 2 \times 2$  super-cells (64 atoms) but, in some cases, additional simulations were also performed on larger super-cells ( $3 \times 3 \times 3$ , i.e. 212 atoms) to control the accuracy of the insertion energy and to confirm atomic positions.  $E_i$  corresponds to the energy needed to insert one H atom in the  $\text{Ti}_3\text{Al}$  system in relation to the  $\text{H}_2$  molecule. It is expressed by:

$$E_i = E_o[\text{Ti}_3\text{Al} + \text{H}] - E_o[\text{Ti}_3\text{Al}] - \frac{1}{2}E_o[\text{H}_2] \quad (2)$$

$E_o$  are the DFT energies of the super-cells,  $E_o[\text{H}_2]$  is the DFT energy of the  $\text{H}_2$  molecule. Results are given in Table 3, for stable configurations only.

After relaxation, nine ‘‘stable’’ positions were found, with no guarantee of them being local minimums. The most stable position is the  $2a$  configuration, the octahedral site composed of Ti atoms only. The other sites exhibit a higher energy. To test the stability, vibrational properties were computed, as seen above, these will help in the analysis. Results show that H atoms preferably occupy sites that are far away from Al atoms. For instance in  $2a$  sites, there are six Ti atoms around the occupancy site; in  $4f$  sites, there are three Ti atoms and one Al,

however the H atom is closer to the Ti atoms, etc. In the case of the  $12j$  configuration the H atom occupies a  $6h$  position after relaxation, distinct to the first configuration considered, see Table 3. To distinguish both configurations,  $6h$  positions were thus labeled  $\dagger$  and  $\ddagger$  in Table 3.

Phonon properties were calculated for all these ‘‘stable’’ configurations. From IFCs on  $2 \times 2 \times 2$  super-cells (i.e. 64 atoms), phonon band-structure along the high-symmetry points of the first Brillouin zone and phonon density-of-states were plotted, see Fig. 3 (stable positions only). Only the octahedral and tetrahedral sites are stable. Unstable cases are configurations where the H atom either occupies the center of triangles ( $2b, 2d, 6h\dagger$  and  $6h\ddagger$  sites), or is located between two nearest-neighbor Ti atoms ( $12i$  sites).  $2b, 2d, 6h\dagger$  and  $6h\ddagger$  positions show indeed one imaginary frequency, and are transition states between stable sites, as seen above.

From IFCs, the zero-point energies (ZPE) of stable configurations,  $H_v$ , were computed.  $H_v$  is given by:

$$H_v = F_v[\text{Ti}_3\text{Al} + \text{H}] - F_v[\text{Ti}_3\text{Al}] - \frac{1}{2}F_v[\text{H}_2] \quad (3)$$

where  $F_v$  are the Helmholtz free energies computed on fine  $\mathbf{q}$ -mesh grids (i.e.  $20 \times 20 \times 20$ ):

$$F_v = -k_B T \ln \mathcal{Z} = k_B T \sum_{\nu=1}^{3N} \int n_{\nu}(\mathbf{q}) \ln \left[ 2 \sinh \left( \frac{\hbar \omega_{\nu, \mathbf{q}}}{2k_B T} \right) \right] d\mathbf{q} \quad (4)$$

$\omega_{\nu, \mathbf{q}}$  are the frequencies in the wave vector  $\mathbf{q}$  and the mode  $\nu$ .  $\mathcal{Z}$  is the partition function related to the phonons. At 0K,  $1/2F_v[\text{H}_2]$  is equal to 148 meV. Values are reported in Table 3. As in most systems, phonon enthalpy does not change the relative stability of sites. However, the ZPE of tetrahedral sites ( $4f$  and  $12k$  sites) is high, about 80 meV. This was already observed in the case of hydrogen in Al-fcc [20], where the H atom also occupies tetrahedral sites preferentially. H frequencies are located at high energies, as can be seen on the  $p\text{DOS}$  plots, Fig. 3, this explains the high values of ZPEs.

We can now discuss and compare present results with literature values. The negative low value of hydrogen  $H_i$ , -0.65 eV, is in agreement with experimental observations [3, 4, 46, 47], which suggests that the solubility of hydrogen is higher in the  $\text{Ti}_3\text{Al}$  system than in the  $\text{TiAl-L1}_0$  system in which the theoretical insertion energy was found equal to about -0.06 eV [8]. Kimura [3], for instance, showed that hydrogen solubility follows the Sieverts law [48] and measured a solubility energy equal to -0.57 eV, which is in excellent agreement with the DFT value (-0.65 eV). In comparison, the solubility energy in the Ti-hcp system (-0.41 eV [5]) and in Al-fcc (+0.69 eV [20]) is thus significantly lower than here.

To gain insight on the interactions between the H atom and  $\text{Ti}_3\text{Al}$ , the Bader charge,  $\mathcal{B}$  [49], the charge transfer ( $\Delta\rho = \rho[\text{Ti}_3\text{Al} + \text{H}] - \rho[\text{Ti}_3\text{Al}] - \rho[\text{H}]$ ), the volume of formation ( $\Omega_f$ ), the volume of Voronoï and elastic dipoles were computed for stable positions. Calculated values are summarized in Table 4.

First, results show that the charge transfer is weak and local: the H atom completes its  $s$  shell and gains almost one electron. When the H atom is located in an octahedral site, the

Table 2: Wyckoff positions and site symmetry [24].

$2a$	$2b$	$2d$	$4e$	$4f$	$6g$
(0, 0, 0), (0, 0, 1/2)	(0, 0, 1/4), (0, 0, 3/4)	(1/3, 2/3, 3/4), (2/3, 1/3, 3/4)	(0, 0, $z_e$ ), (0, 0, $z_e+1/2$ ), (0, 0, $-z_e$ ), (0, 0, $-z_e+1/2$ )	(1/3, 2/3, $z_f$ ), (2/3, 1/3, $z_f+1/2$ ), (1/3, 2/3, $-z_f+1/2$ ), (2/3, 1/3, $-z_f$ )	(1/2, 0, 0), (1/2, 0, 1/2) (0, 1/2, 0), (1/2, 1/2, 1/2) (1/2, 1/2, 0), (0, 1/2, 1/2)
$12i$		$12j$		$12k$	
( $x_i$ , 0, 0), ( $x_i$ , $x_i$ , 0), (0, $x_i$ , 1/2), ( $-x_i$ , 0, 0), ( $-x_i$ , $-x_i$ , 0), (0, $-x_i$ , 1/2)	(0, $x_i$ , 0), ( $x_i$ , 0, 1/2), ( $x_i$ , $x_i$ , 1/2), (0, $-x_i$ , 0), ( $-x_i$ , 0, 1/2), ( $-x_i$ , $-x_i$ , 1/2)	( $x_j$ , $y_j$ , 1/4), ( $-x_j+y_j$ , $-x_j$ , 1/4), ( $y_j$ , $x_j+y_j$ , 3/4), ( $y_j$ , $x_j$ , 3/4), ( $-x_j$ , $-x_j+y_j$ , 3/4), ( $-x_j+y_j$ , $y_j$ , 1/4)	( $-y_j$ , $x_j-y_j$ , 1/4), ( $-x_j$ , $-y_j$ , 3/4), ( $x_j-y_j$ , $x_j$ , 3/4), ( $x_j-y_j$ , $-y_j$ , 3/4), ( $-y_j$ , $-x_j$ , 1/4), ( $x_j$ , $x_j-y_j$ , 1/4)	( $x_k$ , $2x_k$ , $z_k$ ), ( $x_k$ , $-x_k$ , $z_k$ ), ( $2x_k$ , $x_k$ , $z_k+1/2$ ), ( $2x_k$ , $x_k$ , $-z_k$ ), ( $-x_k$ , $x_k$ , $-z_k$ ), ( $x_k$ , $2x_k$ , $-z_k+1/2$ )	( $-2x_k$ , $-x_k$ , $z_k$ ), ( $-x_k$ , $-2x_k$ , $z_k+1/2$ ), ( $-x_k$ , $x_k$ , $z_k+1/2$ ), ( $-x_k$ , $-2x_k$ , $-z_k$ ), ( $-2x_k$ , $-x_k$ , $-z_k+1/2$ ), ( $x_k$ , $-x_k$ , $-z_k+1/2$ )

Table 3: Insertion energy ( $E_i$ , in eV), zero-point energy ( $H_v$ , in meV) and enthalpy of insertion ( $H_i$ , in eV) of a hydrogen atom in different “stable” configurations (see text).

	nb atom	$2a=4e$	$2b$	$2d$	$4f$	$6g$	$6h^\dagger$	$12i$	$12j \approx 6h^\ddagger$	$12k$
		-	-	-	$z_f=0.846$	-	$x_h=0.499$	$x_i=0.297$	$x_j=0.167$	$x_k=0.167$
		-	-	-	-	-	-	-	-	$y_k=0.138$
$E_i$	64	-0.677	+0.318	-0.214	-0.248	-0.159	+0.585	+0.689	-0.043	-0.166
	212	-0.673	-	-	-0.245	-0.155	-	-	-	-0.160
$H_v$		28	unstable	unstable	82	9	unstable	unstable	unstable	78
$H_i$		-0.645	-	-	-0.163	-0.146	-	-	-	-0.082
$\Delta H$		0.0	-	-	0.482	0.499	-	-	-	0.563

Table 4: Calculated values of the Bader charge of H, Al (in first-nearest neighboring position of the H atom) and Ti (also in 1NN of H) atoms ( $\mathcal{B}$ , in  $e^-$ ), volume of formation ( $\Omega_f$ , in  $\text{\AA}^3$ ), the difference between the volume of Voronoi filled and empty ( $\delta\mathcal{V}_v$ , in  $\text{\AA}^3$ ), the volume of relaxation ( $\Omega_r$ , in  $\text{\AA}^3$ , see text) and the elastic dipoles ( $\mathcal{P}_{ij}$ , in eV).  $E_d$  (in meV) corresponds to half of the energy of interaction with its periodic images. The volume of Voronoi of the empty sites are equal to 11.8, 9.8, 11.7 and 9.9  $\text{\AA}^3$  for  $2a$ ,  $4f$ ,  $6g$  and  $12k$  sites respectively. The number of electrons of each specie used in the pseudo-potential (labeled  $\dagger$ ), and the Bader charge of Al and Ti in  $\text{Ti}_3\text{Al-}D0_{19}$  (labeled  $\ddagger$ ) are also given.

		$2a$	$4f$	$6g$	$12k$
$\mathcal{B}$	H (1 $\dagger$ )	1.8	1.9	1.8	1.9
	Al-1NN (3 $\dagger$ , 4.1 $\ddagger$ )	4.1	3.7	3.7	3.6
	Ti-1NN (10 $\dagger$ , 9.6 $\ddagger$ )	9.6	9.6	9.6	9.6
$\Omega_f$		0.88	3.23	1.30	2.93
$\delta\mathcal{V}_v$		0.24	0.64	0.30	0.60
$\mathcal{P}_{ij}$		$\begin{bmatrix} 1.2 & 0.0 & 0.0 \\ 0.0 & 1.2 & 0.0 \\ 0.0 & 0.0 & 0.2 \end{bmatrix}$	$\begin{bmatrix} 1.4 & 0.0 & 0.0 \\ 0.0 & 1.4 & 0.0 \\ 0.0 & 0.0 & 0.6 \end{bmatrix}$	$\begin{bmatrix} 1.7 & 0.6 & -0.1 \\ 0.6 & 1.0 & -0.2 \\ -0.1 & -0.2 & 0.9 \end{bmatrix}$	$\begin{bmatrix} 2.3 & -0.1 & -0.05 \\ -0.1 & 1.2 & -0.1 \\ -0.05 & -0.1 & 0.8 \end{bmatrix}$
$\Omega_r$		1.17	3.41	1.64	3.09
$E_d$		1	4	1	2

charge transfer is smaller than when it is located in a tetrahedral site. The presence of a surrounding Al atom modifies the charge transfer. The Al atom gives part of its electrons, that which can be seen as a destabilization of the bonds around the hydrogen.

These data are complemented by charge transfer plots, Fig. 4. Only one positive (yellow) and one negative (red) iso-surfaces are represented. When an Al atom is located in the first-nearest-neighboring position, a directional charge transfer can be observed from Al to H, in agreement with previous results. In octahedral sites, the charge transfer is more isotropic and smaller, especially in the  $2a$  configurations. The electronic density-of-

states, depicted in Fig. 5, helps understanding the difference between  $2a$  sites and the other stable positions. By comparing the  $eDOS$  of the insertion in  $2a$  sites and the  $eDOS$  of all other configurations, it can be noted that the peak ( $-7.5\text{eV}$ ) associated with the hybridization between hydrogen  $s$ -shells and surrounding atoms is split into two parts when an Al atom is in the vicinity of the H atom: (i) one peak around  $-4.5\text{eV}$ , and (ii) another around  $-8\text{eV}$ . This hybridization explains why H atoms preferably occupy  $2a$  sites.

Elastic distortions induced by the insertion of an H atom were then quantified using the volume of formation,  $\Omega_f$  and the

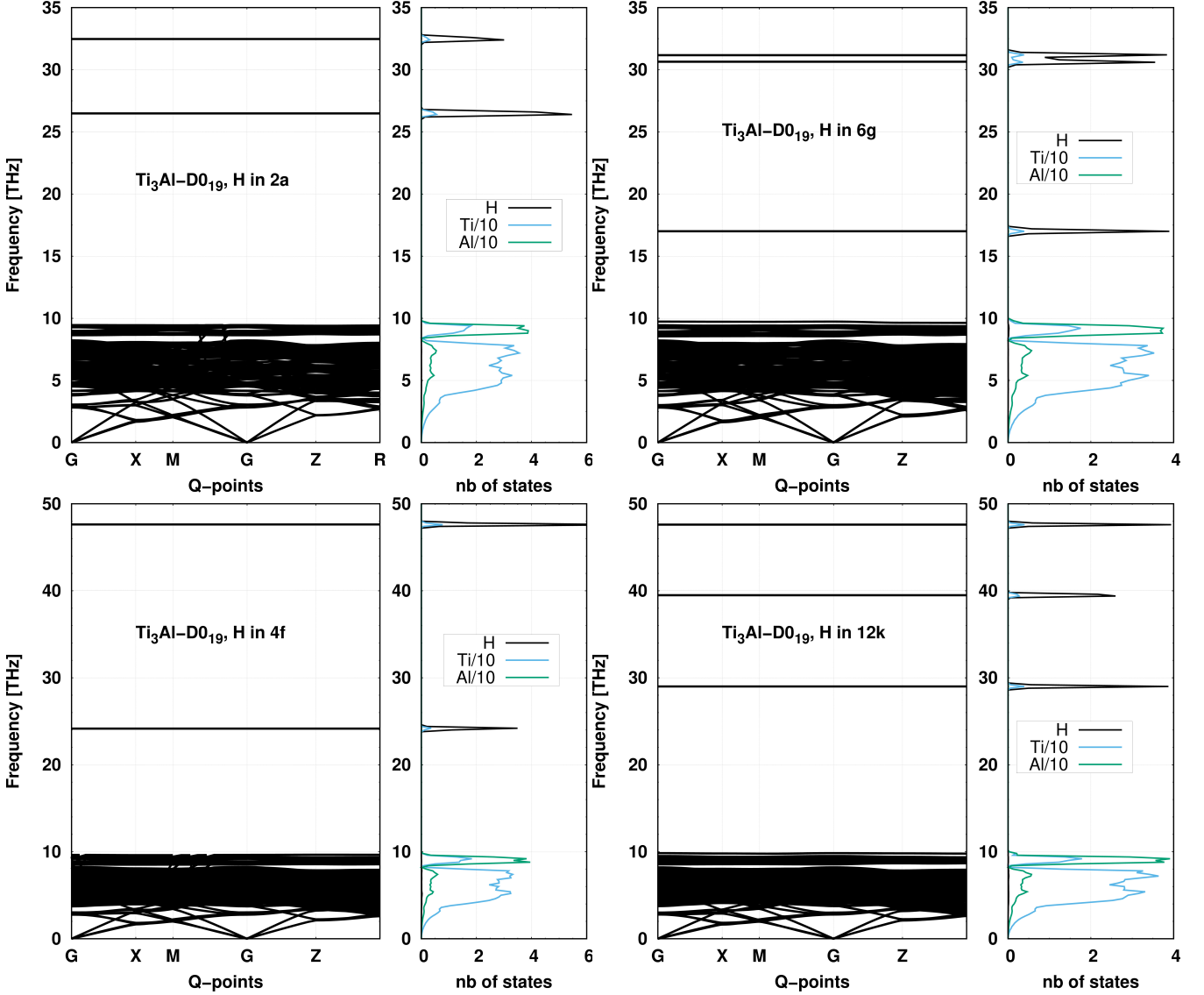


Figure 3: Phonon band structure (*pBAND*) and density-of-states (*pDOS*) of H in *2a*, *4f*, *6g* and *12k* sites. Frequencies are expressed in THz.

volume of Voronoï,  $\delta\mathcal{V}_v$ .  $\Omega_f$  is given by:

$$\Omega_f = V[Ti_3Al + H] - V[Ti_3Al] \quad (5)$$

where  $V$  is the volume of the super-cell with  $(Ti_3Al + H)$  and without  $(Ti_3Al)$  the H atom, and  $\delta\mathcal{V}_v$  is expressed by:

$$\delta\mathcal{V}_v = \mathcal{V}[Ti_3Al + H] - \mathcal{V}[Ti_3Al]. \quad (6)$$

$\mathcal{V}[Y]$  are the volumes of Voronoï of the  $Y$  system calculated with and without hydrogen.  $\delta\mathcal{V}_v$  and  $\Omega_f$  characterize respectively the local and global steric effects due to insertion. Both volumes indicate that hydrogen insertion only induces a local (and weak) strain in the system. For *2a* sites, the elastic distortion is minimal and only local. The effect is mainly due to the electronic hybridization between H atoms and the metal.

In addition, elastic dipole tensors,  $\mathcal{P}_{ij}$  were computed on  $2 \times 2 \times 2$  super-cells. They were deduced from residual stresses when an H atom is inserted in the ideal  $Ti_3Al$  structure and

from the elastic constants of the  $Ti_3Al$  system (given in Table 1). The method proposed by Varvenne *et al.* [50] was used here. The components of  $\mathcal{P}_{ij}$  are found minimal for the octahedral sites. Nonetheless, in all stable sites, hydrogen does not induce a strong strain in the system, this agrees with the conclusion of the previous paragraph. This can be quantified by using relaxation volumes,  $\Omega_r$ . Both values,  $\Omega_r$  and  $\Omega_f$ , are found in excellent agreement. The elastic model confirms firstly that the long range elastic interactions are weak, and secondly, that the model is able to capture elastic relaxations easily. Furthermore, the interaction energies with periodic images are found very small, less than 2meV. This confirms that calculations from small-size boxes and constant volume simulations accurately reproduce insertion energies.

In conclusion, these results show that when a hydrogen atom is inserted into a *2a* site, the strain on the system as well as the electronic interactions are minimized.

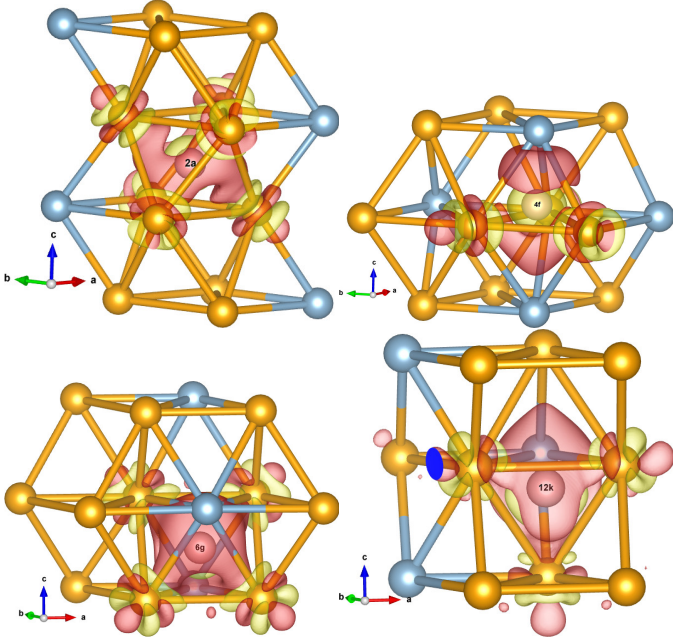


Figure 4: Charge transfer,  $\Delta\rho$ , when sites are filled (from left to right): H in  $2a$ ,  $4f$ ,  $6g$  and  $12k$  sites. Al atoms are in blue and Ti atoms in orange. Charge transfers in red (resp. yellow) correspond to a negative  $\Delta\rho$  (resp. positive  $\Delta\rho$ ).

## 5. Hydrogen diffusivity

The mechanism of diffusion will now be discussed. Jumps between stable sites only were considered, i.e. between  $2a$ ,  $4f$ ,  $6g$  and  $12k$  sites. Amounting to seven distinct jumps, as shown in Fig. 6:  $2a$ - $2a$ ,  $2a$ - $12k$ ,  $4f$ - $4f$ ,  $4f$ - $6g$ ,  $6g$ - $6g$ ,  $6g$ - $12k$  and  $12k$ - $12k$ . The “bonds” between interstitial sites drawn in Fig. 6 represent the shortest jumps. In addition to these cases, two jumps were considered but not drawn: direct jumps between two first-nearest neighboring (1NN)  $2a$  sites and between two 1NN  $6g$  sites along the  $z$  direction. Some jumps in the basal planes were neglected, indeed, H atoms have to go through Ti-Al or Ti-Ti bonds. These configurations should be two second-order transition states, each bond is connected/shared with four stable insertion sites. Since the  $DO_{19}$  structure can be divided into two octahedral and two tetrahedral volumes sharing their triangular faces, the transition states are thus located either at or near the center of gravity of the triangles of the faces of the octahedral and tetrahedral volumes, or in the middle of the Ti-Ti/Ti-Al bonds. However, for the same reasons mentioned in the case of the fcc system [51], when an H atom is in the middle of a Ti-Ti (or Ti-Al) bond, it is located between four stable positions: these are either stable sites, as seen in other systems [43, 44, 52] (which is not the case here), or second-order transition states, and their phonon band-structures are characterized by two imaginary frequencies. In the cases studied here, such configurations always show two imaginary frequencies. For instance, the direct path between two 1NN  $6g$  in the basal plan (or between  $2a$ - $6g$  sites in the basal plan) goes necessarily through a Ti-Ti bond. The transition state is therefore of second-order (confirmed by simulations).

By analyzing the different paths and the results of the inser-

tion, the transition state of each of the four symmetric jumps was identified (see Table 3): (i) the transition state between two 1NN  $12k$  positions is the  $6h\ddagger$  site, (ii) between two 1NN  $4f$  sites, it is the  $2d$  site, (ii) between two 2NN  $2a$  sites, it is the  $2b$  site, and (iv) between two 1NN  $6g$ , it is the  $6h\ddagger$  site. As seen previously phonon results showed that when the H atom is in one of these configurations, the site is unstable (one imaginary frequency associated with H). The site is thus a transitions state for H. For the three jumps remaining, NEB calculations were performed. Results are displayed in Fig. 7 and migration energies are listed in Table 5.

Table 5: Migration energies ( $E_{xy}^m$ , in meV) of jumps from  $x$  to  $y$ . In brackets, Wyckoff positions are given.

$y \setminus x$	$2a$	$4f$	$6g$	$12k$
$2a$	964 ( $2b$ )	-	-	111
$4f$	-	34 ( $2d$ )	436	-
$6g$	-	525	744 ( $6h\ddagger$ )	525
$12k$	622	-	518	123 ( $6h\ddagger$ )

In most cases, migration energies are in the same energy range, i.e. [0.5; 1] eV. The highest migration energy is found for the jump between  $2a$  sites, in the  $z$  direction. Nevertheless, two paths have very low barrier energies: between two 1NN tetrahedral sites ( $4f$ - $4f$  and  $12k$ - $12k$ ), where the jumps are the shortest.

The IFCs of the transition states were systematically computed to verify the nature of the transition state and to calculate  $\Gamma_{xy}$ , see Appendix B. The probability of leaving a site is given by the jump rate,  $\Gamma_{xy}$ , expressed as:

$$\Gamma_{xy}[T] = \frac{k_B T}{h} \frac{\mathcal{Z}_{TS}}{\mathcal{Z}_{EI}} e^{-E_{xy}^m/k_B T} \quad (7)$$

where  $E_{xy}^m$  corresponds to the migration energy given in Table 5.  $\mathcal{Z}_{TS}$  is the vibrational partition function of the transition state and  $\mathcal{Z}_{EI}$  is the partition function of the initial position.  $\mathcal{Z}$  is expressed by eq. (4).

Using these results, the Eyring transition state theory [53] and the multi-site theory proposed by Landman [14, 15], the hydrogen diffusion coefficients were expressed and computed. The diffusion coefficients should depend on ten components:  $\Gamma_{aa}^z$ ,  $\Gamma_{ff}^z$ ,  $\Gamma_{gg}^z$ ,  $\Gamma_{kk}^z$ ,  $\Gamma_{fg}^z$ ,  $\Gamma_{gf}^z$ ,  $\Gamma_{ak}^z$ ,  $\Gamma_{ka}^z$ ,  $\Gamma_{fg}^z$  and  $\Gamma_{gf}^z$ . However, because of the complexity of the elementary processes, the diffusion coefficient equations were not developed in the general case. Nevertheless, two sets of simplified equations were obtained, see Appendix C. Kinetic-Monte-Carlo simulations, including all paths and jumps, were then performed so as to validate models.

Using DFT values, hydrogen diffusion coefficients in the basal plan and perpendicularly,  $D_x$  and  $D_z$ , were calculated as a function of temperature. Results are displayed in Fig. 8. First, both sets of equations, which involve disregarding  $12k$  and/or  $4f$  sites, almost lead to the same results. KMC simulations that include all paths and all jumps, are found in excellent agreement with the models. Because of low barrier energies between  $4f$ - $4f$  and  $12k$ - $12k$  sites, the model accurately reproduces the

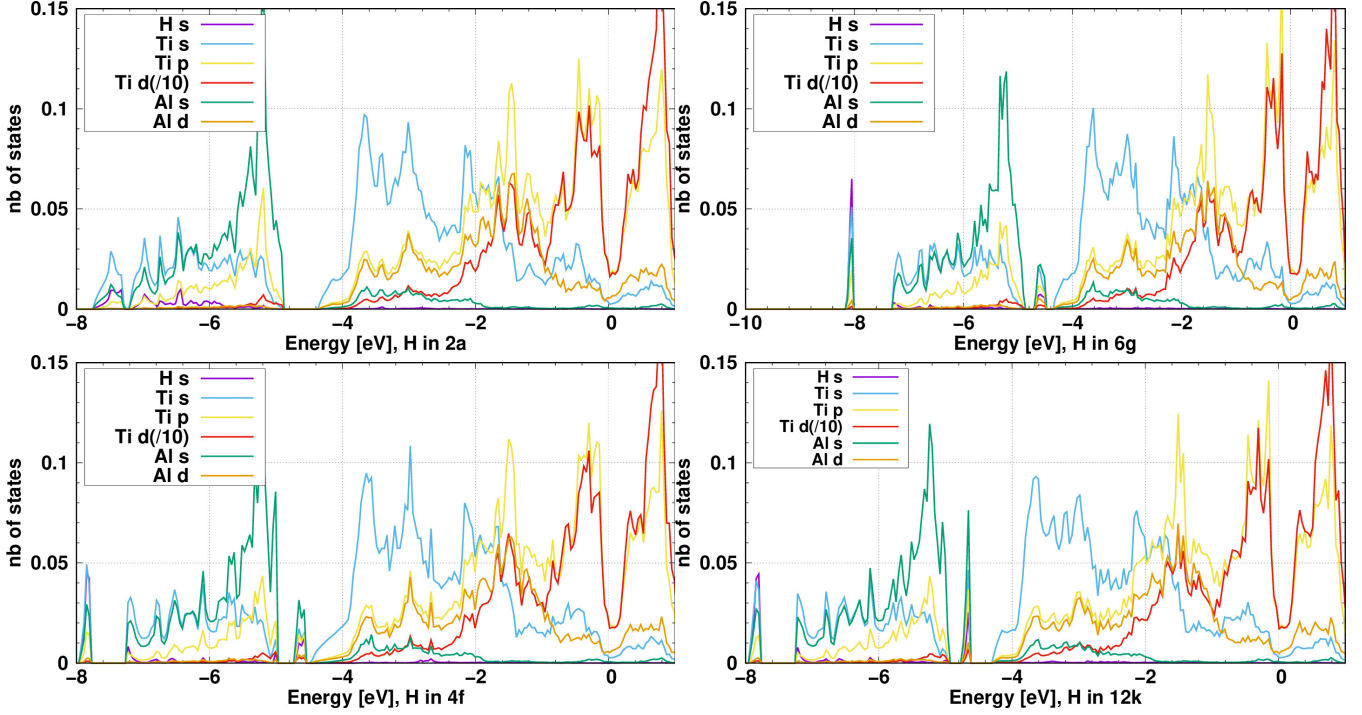


Figure 5: Electronic density-of-states projected onto orbitals and atoms with a hydrogen atom in (from top to bottom)  $2a$ ,  $6g$ ,  $4f$  and  $12k$  sites.

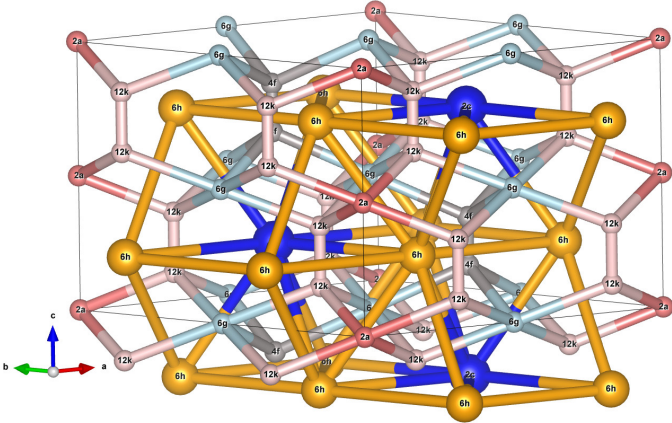


Figure 6: Schematic representation of the network formed by the stable hydrogen insertion sites in the  $\text{Ti}_3\text{Al}$  structure. Jumps are depicted as bonds between interstitial sites, i.e.  $2a$ ,  $4f$ ,  $6g$  and  $12k$ . The bonds are plotted for distances smaller than  $2 \text{ \AA}$ .

complexity of the mechanism. This comparison is a means to further validate the proposed equations on one hand as well as the different coefficients thereby obtained.

An Arrhenius fit was applied to  $D_x$  and  $D_z$ , i.e.  $D[T] = D_o \exp(-E_a/k_B T)$ , to obtain  $D_o$  and  $E_a$ , the activation energies (for both models and kMC simulations). Parameters are given in Table 6 and compared with experimental literature [9].

The Hydrogen diffusion is thus found strongly anisotropic in the  $\text{Ti}_3\text{Al}$  system, even at high temperatures. It can also be noted that H atoms diffuse faster in the  $z$  direction than in the basal plan, contrary to what happens in  $\alpha\text{-TiAl}$ . Miyoshi [9] and Naito [10] measured experimentally a mean diffusion coef-

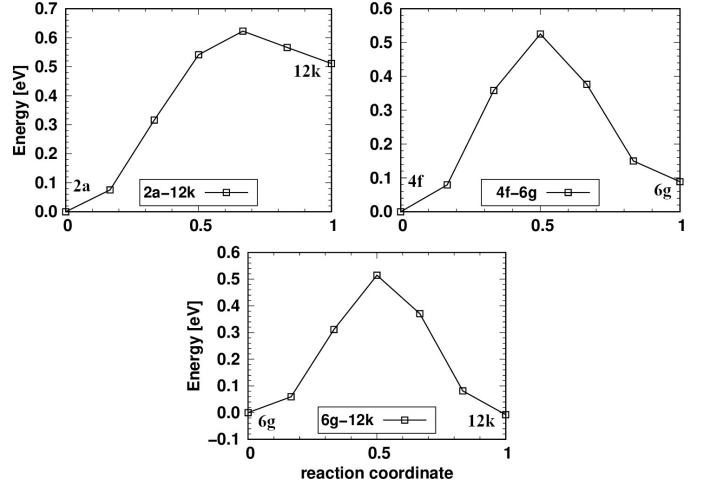


Figure 7: NEB calculations for H atoms, along three paths:  $2a$ - $12k$ ,  $4f$ - $6g$  and  $6g$ - $12k$ .

ficient. Their values are in excellent agreement with our results, see Fig. 8 and Table 6. In order to further improve our theory/experiment comparison, average diffusion coefficients were extracted from kMC simulations and added to in Fig. 8, purple triangle. Values are obviously in excellent agreement with theoretical data. Nonetheless, the model used here is able to capture the anisotropy of the diffusion mechanism in the  $\text{Ti}_3\text{Al}$  system as well.

The diffusivity of hydrogen in  $\text{Ti}_3\text{Al}$  can now be compared with that in other systems:  $\text{Ti-hcp}$  and  $\text{TiAl-L1}_0$  systems. The diffusion coefficients of H in  $\text{TiAl-L1}_0$  (presented in the Ref. [8]), those of H in  $\text{Ti-hcp}$  (computed using data given in Ref.

Table 6: Activation energies ( $E_a$ , in eV) and  $D_o$  (in  $10^{-6}$  m<sup>2</sup>/s) obtained from an Arrhenius fit. Values labeled <sup>1</sup> correspond to the fit for the first set of equations and <sup>2</sup> for the second.

direction	Ti <sub>3</sub> Al		TiAl [8]		Ti	
	$E_a$	$D_o$	$E_a$	$D_o$	$E_a$	$D_o$
$x, y$	1.043 <sup>1</sup> /1.043 <sup>2</sup> /1.00 <sup>kmc</sup>	19.68 <sup>1</sup> /26.54 <sup>2</sup> /22.26 <sup>kmc</sup>	0.537	1.58	0.446	0.51
$z$	0.716 <sup>1</sup> /0.723 <sup>2</sup> /0.739 <sup>kmc</sup>	5.88 <sup>1</sup> /6.53 <sup>2</sup> /3.76 <sup>kmc</sup>	0.811	3.04	0.431	0.74
Exp.	0.838±0.128 [9]		5.0		0.449±0.078 [9]	

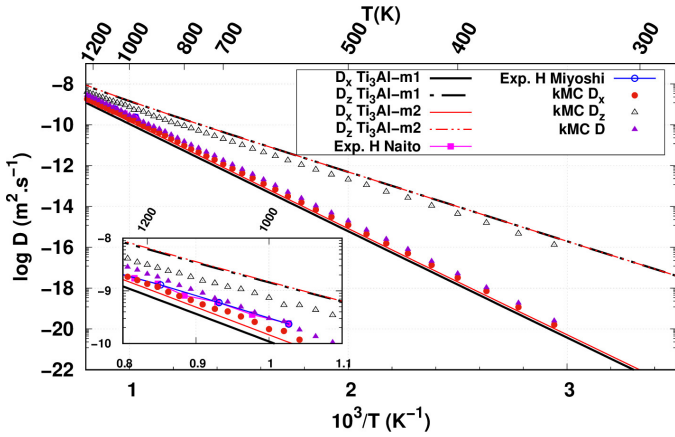


Figure 8: Diffusion coefficients of H atoms in the Ti<sub>3</sub>Al system.  $D_x$ ,  $D_z$  are plotted as a function of  $1/T$ . Both models (labeled m1 and m2) are plotted, as well as kMC simulations. Experimental data, extracted from the works of Naito [10] and Miyoshi [9], are also represented.

[5]), and equations (D.1) and (D.2) given in Appendix D are plotted in Fig. 9 for comparison. For Ti-hcp, the processes are simpler than in the case of oxygen [43], the expressions of  $D$  were thus easily determined.

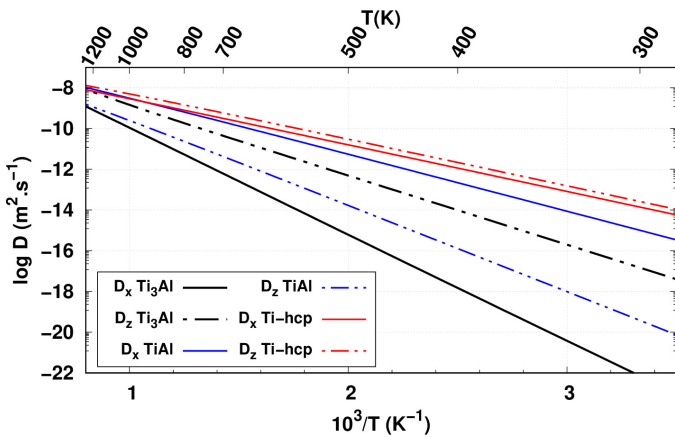


Figure 9: Hydrogen diffusion coefficients in TiAl systems as a function of  $1/T$ .

From Ti, to TiAl, to Ti<sub>3</sub>Al, anisotropy increases. Hydrogen diffusion, however, is slower. Opposite behaviors can be noticed: hydrogen diffusivity is slower in Ti<sub>3</sub>Al than in TiAl and Ti-hcp systems, even though its solubility (should be/is) higher. In fine, the flux of hydrogen should be equivalent in TiAl and Ti<sub>3</sub>Al. To explain the differences between the two TiAl systems, it can be noted that the presence of aluminum atoms leads to a

significant increase in energy barriers and consequently, results in a slower diffusion of hydrogen. The fact that H diffuses more slowly in Ti<sub>3</sub>Al than in TiAl can be explained by the important stability of the insertion site ( $2a$ ) in Ti<sub>3</sub>Al. This stable site could behave as a trap in which the H atom has difficulty moving. The solubility is lower in TiAl, but the energy difference between sites is smaller, thereby facilitating the diffusion of hydrogen.

## 6. Conclusion

This manuscript is a complete study of the insertion and diffusion of hydrogen in the intermetallic Ti<sub>3</sub>Al-DO<sub>19</sub> system. DFT simulations show that H atoms preferentially occupy  $2a$  sites. The system admits three additional stable configurations:  $6g$ ,  $4f$  and  $12k$  sites, which are nonetheless higher in energy than  $2a$  sites. H atoms prefer to occupy the sites surrounded by Ti atoms, with which they have a better affinity. Elastic and electronic effects show a low interaction between hydrogen and the metal.

Trajectories in the Ti<sub>3</sub>Al network were meticulously studied at the atomic scale. The energy landscape of the H atom in the Ti<sub>3</sub>Al system is found complex, exhibiting many jumps and migration energies of different orders of magnitude. So as to model the diffusion, two sets of simplified equations were determined and comparison with kMC simulations was successful. Calculated hydrogen diffusion coefficients were then compared with H diffusion coefficients in the Ti-hcp and TiAl-L1<sub>0</sub> systems. Results show that H diffusion is slow and highly anisotropic in the Ti<sub>3</sub>Al-DO<sub>19</sub> system.

## Acknowledgments

This work was performed using HPC resources from CALMIP (Grant 2019-p0912). The author is grateful to A. Prillieux and D. Tanguy for their comments. He also thanks N. Renon and E. Courcelle (CALMIP technical support), and K. Alloula (EN-SIACET) for their help. Some figures were generated with VESTA software [54].

## Appendix A. Heat capacity of the Ti<sub>3</sub>Al system

For information purposes, the heat capacity at constant volume,  $C_v$ , expressed by:

$$C_v(T) = -T \frac{\partial^2 F_{vib}}{\partial T^2} \Big|_V = -k_B \sum_{\mathbf{q}, \nu} \left( \frac{\hbar \omega_{\mathbf{q}, \nu}}{2k_B T} \right)^2 \frac{1}{\sinh^2 \left( \frac{\hbar \omega_{\mathbf{q}, \nu}}{2k_B T} \right)} \quad (\text{A.1})$$

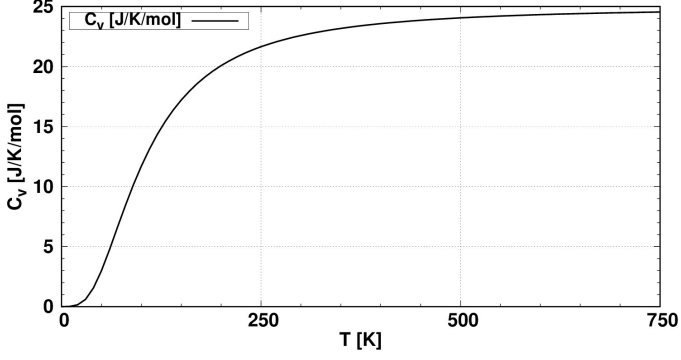


Figure A.10: Evolution of heat capacity,  $C_v$ , (in  $\text{J K}^{-1} \text{mol}^{-1}$ ) of the  $\text{Ti}_3\text{Al-D019}$  system as a function of  $T$ .

is reported here and plotted in Fig. A.10. The Debye temperature,  $\theta_D$ , given by:

$$C_v = 9N_B \left(\frac{T}{\theta_D}\right)^3 \int_0^{\theta_D/T} \frac{x^4 e^x}{(e^x - 1)^2} dx \quad (\text{A.2})$$

is equal to 10.24 THz, i.e. 499K.

## Appendix B. Jump rates

The attempt frequency of each jump studied is plotted in Fig. B.11. They were computed using the migration energies summarized in Table 5 and Helmholtz vibration energies.  $\Gamma_{ka}$ ,

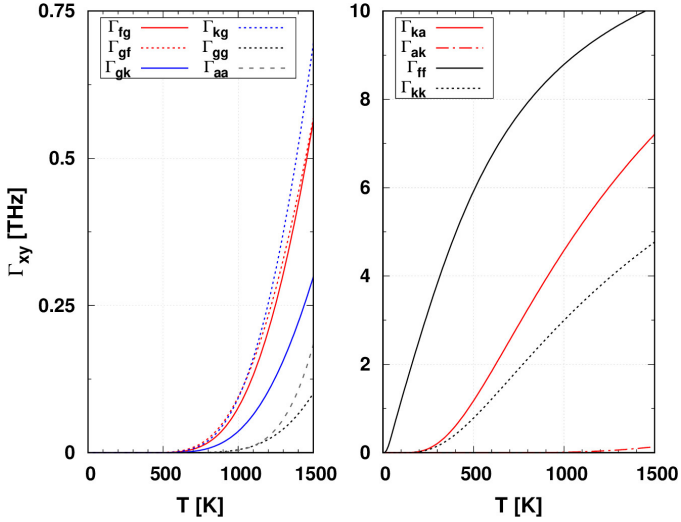


Figure B.11: Attempt frequencies of jumps as a function of  $T$ :  $\Gamma_{aa}$ ,  $\Gamma_{ff}$ ,  $\Gamma_{gg}$ ,  $\Gamma_{kk}$ ,  $\Gamma_{fg}$ ,  $\Gamma_{gf}$ ,  $\Gamma_{ak}$ ,  $\Gamma_{ka}$ ,  $\Gamma_{fg}$  and  $\Gamma_{gf}$ .

$\Gamma_{ff}$  and  $\Gamma_{kk}$  are one order of magnitude higher than the other rates.

## Appendix C. Multi-sites model

Regarding hydrogen in the  $\text{Ti}_3\text{Al}$  system, four sites were identified as stable, i.e. 24 sites per unit-cell ( $2a$ ,  $4f$ ,  $6g$  and  $12k$ ). This cannot be solved using Landman's method [14, 15],

indeed it implies manipulating formally an immense matrix ( $24 \times 24$ ). Nevertheless, different approximation were made so as to propose simplified equations.

For simplification purposes,  $12k$  sites were first considered as transition states between  $2a$  and  $6g$  sites. As a result, the size of the system to be solved is reduced. New jump attempts were then introduced: (i)  $\Gamma_{akg}$  and  $\Gamma_{gka}$  the probability to jump between a  $2a$  and a  $6g$  site through a  $12k$  site, (ii)  $\Gamma_{gkg}$  and  $\Gamma_{aka}$  between two 1NN  $2a$  or  $6g$  through a  $12k$  site. In this approximation, the paths were always considered, but not the  $12k$  sites. Hydrogen diffusion coefficients,  $D$ , are thus expressed as:

$$D_{x,y}[T] = \frac{a^2}{4} \frac{\Gamma_{akg}\Gamma_{fg}(\Gamma_{gf} + 12\Gamma_{gka} + 6\Gamma_{gkg})}{(3\Gamma_{akg}\Gamma_{fg} + 2\Gamma_{akg}\Gamma_{gf} + 2\Gamma_{fg}\Gamma_{gka})} \quad (\text{C.1})$$

in the basal plan, and:

$$D_z[T] = \frac{c^2}{4} \Gamma_{fg} \left( 3\Gamma_{akg}\Gamma_{ff}\Gamma_{gf} + 6\Gamma_{akg}\Gamma_{ff}\Gamma_{gg}^z + 9\Gamma_{akg}\Gamma_{fg}\Gamma_{gg}^z + 4\Gamma_{aa}^z\Gamma_{ff}\Gamma_{gka} + 12\Gamma_{aka}\Gamma_{ff}\Gamma_{gka} + 12\Gamma_{akg}\Gamma_{ff}\Gamma_{gka} + 6\Gamma_{aa}^z\Gamma_{fg}\Gamma_{gka} + 18\Gamma_{aka}\Gamma_{fg}\Gamma_{gka} + 18\Gamma_{akg}\Gamma_{fg}\Gamma_{gka} + 24\Gamma_{akg}\Gamma_{ff}\Gamma_{gkg} + 36\Gamma_{akg}\Gamma_{fg}\Gamma_{gkg} \right) / \left( (3\Gamma_{akg}\Gamma_{fg} + 2\Gamma_{akg}\Gamma_{gf} + 2\Gamma_{fg}\Gamma_{gka})(2\Gamma_{ff} + 3\Gamma_{fg}) \right) \quad (\text{C.2})$$

along  $z$ .  $a$  and  $c$  are the lattice parameters of the  $\text{Ti}_3\text{Al}$  system. To compute the new attempt frequency, approximations were made and migration energies were simplified, see Table C.7.

Table C.7: Migration energies ( $E_{x-y}^m$ , in meV) of jumps from  $x$  to  $y$  for the first model.  $E_m^{aka} = E_m^{ak} + E_m^{kk} - E_m^{ka}$ ,  $E_m^{akg} = E_m^{ak} - E_m^{ka} + E_m^{kg}$ ,  $E_m^{gka} = E_m^{gk} + E_m^{ka} - E_m^{ga}$ ,  $E_m^{gkg} = E_m^{gk}$

$y \setminus x$	$2a$	$4f$	$6g$
$2a$	964 (2b)/634 (12k)	-	518 (12k)
$4f$	-	34 (2d)	436
$6g$	1038 (12k)	525	744 (6h <sup>†</sup> )/744 (12k)

In the second approximation,  $4f$  and  $12k$  sites were both disregarded. To complement the previous simplification, an additional jump rate was introduced,  $\Gamma_{gfg}$ . The trajectory through the  $4f$  and  $12k$  sites were always all included. The diffusion coefficient in the basal plan,  $D_x$ , is thus given by:

$$D_{x,y}[T] = \frac{a^2}{2} \frac{3\Gamma_{akg}(\Gamma_{gfg} + 2\Gamma_{gka} + \Gamma_{gkg})}{(3\Gamma_{akg} + 2\Gamma_{gka})} \quad (\text{C.3})$$

and along  $z$ :

$$D_z[T] = \frac{c^2}{4} \left( 9\Gamma_{akg}\Gamma_{gfg} + 3\Gamma_{akg}\Gamma_{gg}^z + 2\Gamma_{aa}^z\Gamma_{gka} + 6\Gamma_{aka}\Gamma_{gka} + 6\Gamma_{akg}\Gamma_{gka} + 12\Gamma_{akg}\Gamma_{gkg} \right) / \left( 3\Gamma_{akg} + 2\Gamma_{gka} \right) \quad (\text{C.4})$$

To compute  $\Gamma_{gfg}$ , the limiting step is the jump from  $4f$  to  $6g$ , see values in Table C.8.

Table C.8: Migration energies ( $E_m^{x-y}$ , in meV) of jumps from  $x$  to  $y$  for the second model.  $E_m^{aka} = E_m^{ak} + E_m^{kk} - E_m^{ka}$ ,  $E_m^{akg} = E_m^{ak} - E_m^{ka} + E_m^{kg}$ ,  $E_m^{gkg} = E_m^{gk} - E_m^{kg} + E_m^{kk}$ ,  $E_m^{gka} = E_m^{gk}$  and  $E_m^{gfg} = E_m^{fg}$ .

$y \setminus x$	$2a$	$6g$
$2a$	964 (2b)/634 (12k)	518 (12k)
$6g$	1038 (12k)	744 (6h <sup>+</sup> )/744 (12k)/525 (4f)

#### Appendix D. Hydrogen diffusion coefficient in the Ti-hcp structure

In the Ti-hcp system (space group 194, Ti atoms in  $2c$  positions), where H atoms can only occupy octahedral ( $2a$ ) sites and tetrahedral ( $4f$ ) sites [5, 7], the diffusion coefficients are expressed as:

$$D_{x,y}[T] = \frac{a^2}{2} \cdot \frac{(3\Gamma_{aa}^x + 2\Gamma_{af})\Gamma_{fa}}{2\Gamma_{af} + \Gamma_{fa}} \quad (\text{D.1})$$

$$D_z[T] = \frac{c^2}{4} \cdot \frac{(3\Gamma_{aa}^z\Gamma_{fa} + 2\Gamma_{aa}^z\Gamma_{ff} + 3\Gamma_{af}\Gamma_{ff})\Gamma_{fa}}{(2\Gamma_{af} + \Gamma_{fa})(3\Gamma_{fa} + 2\Gamma_{ff})} \quad (\text{D.2})$$

The notations are depicted in Fig. D.12. The construction of

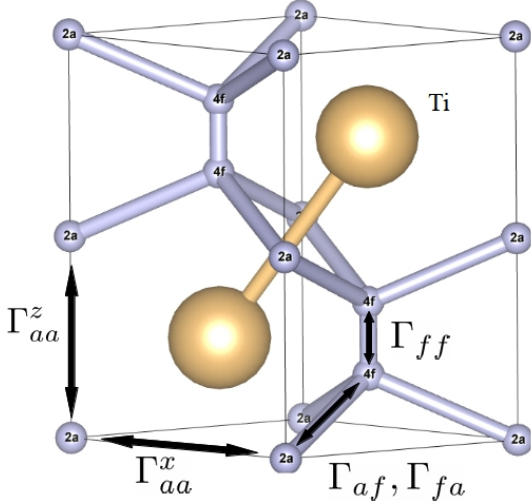


Figure D.12: Schematic representation of H paths and attempt frequency in the Ti-hcp system.

Landman [14, 15] was used. Two quantities are required: the Laplace transform of the waiting time density matrix,  $\underline{\psi}(u)$ , and the Fourier transform matrix of the displacements of hydrogen in TiAl,  $\underline{p}(k)$ .  $\underline{\psi}(u)$  is given by:

$$\underline{\psi}(u) = \begin{matrix} & 2a_1 & 2a_2 & 4f_1 & 4f_2 & 4f_3 & 4f_4 \\ \begin{matrix} 2a_1 \\ 2a_2 \\ 4f_1 \\ 4f_2 \\ 4f_3 \\ 4f_4 \end{matrix} & \begin{bmatrix} \frac{6\Gamma_{aa}^x}{K_a} & \frac{2\Gamma_{aa}^z}{K_a} & \frac{3\Gamma_{fa}}{K_f} & 0 & 0 & \frac{3\Gamma_{fa}}{K_f} \\ \frac{2\Gamma_{aa}^x}{K_a} & \frac{6\Gamma_{aa}^z}{K_a} & 0 & \frac{3\Gamma_{fa}}{K_f} & \frac{3\Gamma_{fa}}{K_f} & 0 \\ \frac{3\Gamma_{af}}{K_a} & 0 & 0 & \frac{\Gamma_{ff}}{K_f} & 0 & 0 \\ 0 & \frac{3\Gamma_{af}}{K_a} & \frac{\Gamma_{ff}}{K_f} & 0 & 0 & 0 \\ 0 & \frac{3\Gamma_{af}}{K_a} & 0 & 0 & 0 & \frac{\Gamma_{ff}}{K_f} \\ \frac{3\Gamma_{af}}{K_a} & 0 & 0 & 0 & \frac{\Gamma_{ff}}{K_f} & 0 \end{bmatrix} \end{matrix} \quad (\text{D.3})$$

where  $K_a = 6\Gamma_{af} + 6\Gamma_{aa}^x + 2\Gamma_{aa}^z + u$  and  $K_f = 3\Gamma_{fa} + \Gamma_{ff} + u$ .  $\Gamma_{xy}$  is the probability of escape from internal state  $x$  to another state  $y$ .  $\underline{p}(k)$  is given by:

$$\underline{p}(k) = \begin{matrix} & 2a_1 & 2a_2 & 4f_1 & 4f_2 & 4f_3 & 4f_4 \\ \begin{matrix} 2a_1 \\ 2a_2 \\ 4f_1 \\ 4f_2 \\ 4f_3 \\ 4f_4 \end{matrix} & \begin{bmatrix} A_{a_1a_1} & A_{a_2a_1} & A_{f_1a_1} & 0 & 0 & A_{f_4a_1} \\ A_{a_1a_2} & A_{a_2a_2} & 0 & A_{f_2a_2} & A_{f_3a_2} & 0 \\ A_{a_1f_1} & 0 & 0 & A_{f_2f_1} & 0 & 0 \\ 0 & A_{a_2f_2} & A_{f_1f_2} & 0 & 0 & 0 \\ 0 & A_{a_2f_3} & 0 & 0 & 0 & A_{f_4f_3} \\ A_{a_1f_4} & 0 & 0 & 0 & A_{f_3f_4} & 0 \end{bmatrix} \end{matrix} \quad (\text{D.4})$$

where

$$\begin{aligned} A_{a_1a_1} &= [e^{i l_x k_x} + e^{i l_y k_y} + e^{i(l_y k_y + l_x k_x)} + e^{-i l_x k_x} + e^{-i l_y k_y} + e^{-i(l_y k_y + l_x k_x)}]/6 \\ A_{a_2a_2} &= [e^{i l_x k_x} + e^{i l_y k_y} + e^{i(l_y k_y + l_x k_x)} + e^{-i l_x k_x} + e^{-i l_y k_y} + e^{-i(l_y k_y + l_x k_x)}]/6 \\ A_{a_1a_2} &= A_{a_2a_1} = [1 + e^{i l_z k_z}]/2 \\ A_{f_1a_1} &= [1 + e^{i l_x k_x} + e^{i(l_y k_y + l_x k_x)}]/3 \\ A_{f_4a_1} &= e^{-i l_z k_z} [1 + e^{-i l_y k_y} + e^{i(l_y k_y + l_x k_x)}]/3 \\ A_{f_2a_2} &= A_{f_3a_2} = [1 + e^{i l_x k_x} + e^{i(l_y k_y + l_x k_x)}]/3 \\ A_{f_3f_4} &= A_{f_4f_3} = A_{f_1f_2} = A_{f_2f_1} = 1 \\ A_{a_2f_3} &= A_{a_2f_2} = A_{a_1f_1} = [1 + e^{-i l_x k_x} + e^{-i(l_y k_y + l_x k_x)}]/3 \\ A_{a_1f_4} &= e^{-i l_z k_z} [1 + e^{-i l_x k_x} + e^{-i(l_y k_y + l_x k_x)}]/3 \end{aligned} \quad (\text{D.5})$$

with  $l_x = l_x = a$  and  $l_z = c$ . In order to derive  $D_{x,y}$  and  $D_z$ , the procedure suggested by Landmann [15] and described by Wu [43] was then used.

Ishioka [55] found the same expression directly, when  $\Gamma_{aa}^x = 0$ . Connétable *et al.* [5] explicitly reported the value of each parameter. Using the present notation, it was found that:

$$\begin{aligned} \Gamma_{aa}^x[T] &= 0 \\ \Gamma_{aa}^z[T] &= 8\text{Thz} \cdot \exp(-0.65\text{eV}/k_B T) \\ \Gamma_{ff}[T] &= 22\text{Thz} \cdot \exp(-0.12\text{eV}/k_B T) \\ \Gamma_{af}[T] &= 9\text{Thz} \cdot \exp(-0.46\text{eV}/k_B T) \\ \Gamma_{fa}[T] &= 27\text{Thz} \cdot \exp(-0.39\text{eV}/k_B T). \end{aligned}$$

Diffusion coefficients can thus be compared with the results of Bakulin [6] and experimental measurements. The model allows to refine the values and identify a small anisotropy.

#### References

- [1] I. Robertson, *The effect of hydrogen on dislocation dynamics*, Engineering Fracture Mechanics 68 (6) (2001) 671 – 692 (2001). doi:[https://doi.org/10.1016/S0013-7944\(01\)00011-X](https://doi.org/10.1016/S0013-7944(01)00011-X). URL <http://www.sciencedirect.com/science/article/pii/S001379440100011X>
- [2] S. Lynch, *Hydrogen embrittlement (he) phenomena and mechanisms*, in: Stress Corrosion Cracking, Elsevier, 2011, pp. 90–130 (2011).
- [3] M. Kimura, T. Tsuchiyama, S. Naito, M. Yamamoto, *Faraday communications. solubility of hydrogen and deuterium in ti3al*, Journal of the Chemical Society, Faraday Transactions 90 (9) (1994) 1355–1356 (1994).
- [4] S. Naito, M. Yamamoto, M. Doi, M. Kimura, *Dissolution of hydrogen and deuterium in titanium, ti 94 al 6 and ti 3 al*, Journal of the Chemical Society, Faraday Transactions 91 (13) (1995) 1967–1973 (1995).
- [5] D. Connétable, J. Huez, E. Andrieu, C. Mijoule, *First-principles study of the migration process of hydrogen and vacancy in titanium*, J. Phys.: Condens. Matter 23 (2011) 405401 (2011). URL <http://dx.doi.org/10.1088/0953-8984/23/40/405401>

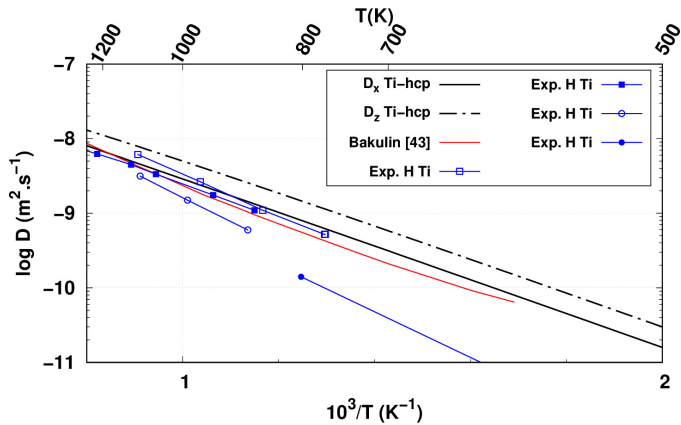


Figure D.13: Diffusion coefficients of H atoms in the Ti-hcp system. Comparison with experimental data and the Bakulin's results [6]. Experimental values were extracted from the work of Bakulin.

- [6] A. Bakulin, T. Spiridonova, S. Kulkova, S. Hocker, S. Schmauder, **Hydrogen diffusion in doped and undoped  $\alpha$ -Ti: An ab-initio investigation**, International Journal of Hydrogen Energy 41 (21) (2016) 9108–9116 (2016). doi:<https://doi.org/10.1016/j.ijhydene.2016.03.192>. URL <http://www.sciencedirect.com/science/article/pii/S0360319916301409>
- [7] Y. Lu, P. Zhang, **First-principles study of temperature-dependent diffusion coefficients: Hydrogen, deuterium, and tritium in  $\alpha$ -Ti**, Journal of Applied Physics 113 (19) (2013) 193502 (2013). arXiv:<https://doi.org/10.1063/1.4805362>, doi:[10.1063/1.4805362](https://doi.org/10.1063/1.4805362). URL <https://doi.org/10.1063/1.4805362>
- [8] D. Connétable, **Theoretical study on hydrogen solubility and diffusivity in the  $\gamma$ -tial  $L1_0$  structure**, International Journal of Hydrogen Energy 44 (2019) 12215–12227 (2019). doi:<https://doi.org/10.1016/j.ijhydene.2019.03.110>.
- [9] T. Miyoshi, S. Naito, M. Yamamoto, M. Doi, M. Kimura, **Diffusion of hydrogen in titanium, ti88al12 and ti3al**, Journal of the Chemical Society, Faraday Transactions 92 (3) (1996) 483–486 (1996).
- [10] S. Naito, O. Hashitomi, M. Yamamoto, Y. Baba, M. Kimura, **Faraday communications. diffusion of hydrogen in ti 3 al**, Journal of the Chemical Society, Faraday Transactions 90 (16) (1994) 2423–2424 (1994).
- [11] S. Naito, M. Yamamoto, M. Doi, M. Kimura, **High-temperature diffusion of hydrogen and deuterium in titanium and ti3al**, Journal of the Electrochemical Society 145 (7) (1998) 2471–2475 (1998).
- [12] X. Shen, D. Connétable, D. Tanguy, **Modeling segregation of hydrogen to the  $\sigma_9 - (221) - [110]$  symmetric tilt grain boundary in al**, Phil. Mag. 94 (2014) 2247–2261 (2014).
- [13] Y. Fukai, **The metal-hydrogen system: basic bulk properties**, Vol. 21, Springer Science & Business Media, 2006 (2006).
- [14] U. Landman, M. F. Shlesinger, **Stochastic theory of multistate diffusion in perfect and defective systems. i. mathematical formalism**, Phys. Rev. B 19 (1979) 6207–6219 (Jun 1979). doi:[10.1103/PhysRevB.19.6207](https://doi.org/10.1103/PhysRevB.19.6207). URL <http://link.aps.org/doi/10.1103/PhysRevB.19.6207>
- [15] U. Landman, M. F. Shlesinger, **Stochastic theory of multistate diffusion in perfect and defective systems. ii. case studies**, Phys. Rev. B 19 (1979) 6220–6237 (Jun 1979). doi:[10.1103/PhysRevB.19.6220](https://doi.org/10.1103/PhysRevB.19.6220). URL <http://link.aps.org/doi/10.1103/PhysRevB.19.6220>
- [16] G. Kresse, J. Hafner, **Ab initio molecular dynamics for liquid metals**, Phys. Rev. B 47 (1993) 558–561 (Jan 1993). doi:[10.1103/PhysRevB.47.558](https://doi.org/10.1103/PhysRevB.47.558). URL <https://link.aps.org/doi/10.1103/PhysRevB.47.558>
- [17] G. Kresse, D. Joubert, **From ultrasoft pseudopotentials to the projector augmented-wave method**, Phys. Rev. B 59 (1999) 1758–1775 (Jan 1999). doi:[10.1103/PhysRevB.59.1758](https://doi.org/10.1103/PhysRevB.59.1758). URL <https://link.aps.org/doi/10.1103/PhysRevB.59.1758>
- [18] P. E. Blöchl, **Projector augmented-wave method**, Phys. Rev. B 50 (1994) 17953–17979 (Dec 1994). doi:[10.1103/PhysRevB.50.17953](https://doi.org/10.1103/PhysRevB.50.17953). URL <https://link.aps.org/doi/10.1103/PhysRevB.50.17953>
- [19] J. P. Perdew, K. Burke, M. Ernzerhof, **Generalized gradient approximation made simple**, Phys. Rev. Lett. 77 (1996) 3865–3868 (Oct 1996). doi:[10.1103/PhysRevLett.77.3865](https://doi.org/10.1103/PhysRevLett.77.3865). URL <https://link.aps.org/doi/10.1103/PhysRevLett.77.3865>
- [20] C. Wolverton, V. Ozolins, M. Asta, **Hydrogen in aluminum: First-principles calculations of structure and thermodynamics**, Phys. Rev. B 69 (2004) 144109 (Apr 2004). doi:[10.1103/PhysRevB.69.144109](https://doi.org/10.1103/PhysRevB.69.144109). URL <https://link.aps.org/doi/10.1103/PhysRevB.69.144109>
- [21] H. J. Monkhorst, J. D. Pack, **Special points for brillouin-zone integrations**, Phys. Rev. B 13 (1976) 5188–5192 (Jun 1976). doi:[10.1103/PhysRevB.13.5188](https://doi.org/10.1103/PhysRevB.13.5188). URL <https://link.aps.org/doi/10.1103/PhysRevB.13.5188>
- [22] G. Henkelman, B. P. Uberuaga, H. Jónsson, **A climbing image nudged elastic band method for finding saddle points and minimum energy paths**, The Journal of Chemical Physics 113 (22) (2000) 9901–9904 (2000). arXiv:<https://doi.org/10.1063/1.1329672>, doi:[10.1063/1.1329672](https://doi.org/10.1063/1.1329672). URL <https://doi.org/10.1063/1.1329672>
- [23] A. Togo, F. Oba, I. Tanaka, **First-principles calculations of the ferroelastic transition between rutile-type and  $cacl_2$ -type  $sio_2$  at high pressures**, Phys. Rev. B 78 (2008) 134106 (Oct 2008). doi:[10.1103/PhysRevB.78.134106](https://doi.org/10.1103/PhysRevB.78.134106). URL <https://link.aps.org/doi/10.1103/PhysRevB.78.134106>
- [24] M. I. Aroyo, J. M. Perez-Mato, C. Capillas, Bilbao crystallographic server: I. databases and crystallographic computing programs, Zeitschrift für Kristallographie - Crystalline Materials 221 (2009) 15–27 (2009). doi:<https://doi.org/10.1524/zkri.2006.221.1.15>.
- [25] J. C. Schuster, M. Palm, **Reassessment of the binary aluminum-titanium phase diagram**, Journal of Phase Equilibria and Diffusion 27 (3) (2006) 255–277 (Jun 2006). doi:[10.1361/154770306X109809](https://doi.org/10.1361/154770306X109809). URL <https://doi.org/10.1361/154770306X109809>
- [26] C. Kittel, **Introduction to Solid State Physics**, Wiley, New York, 1996 (1996).
- [27] Y. Liu, L. Liu, S. Wang, H. Ye, **First-principles study of shear deformation in tial and ti3al**, Intermetallics 15 (2007) 428–435 (2007). doi:[10.1016/j.intermet.2006.08.012](https://doi.org/10.1016/j.intermet.2006.08.012).
- [28] Y. Koizumi, M. Yoshiya, A. Sugihara, Y. Minamino, **Effect of impurity atoms on  $\alpha$ -2/ $\gamma$  lamellar interfacial misfit in ti–al alloy: a systematic first principles study**, Philosophical Magazine 91 (2011) 3685–3704 (2011).
- [29] W. Pearson, **A Handbook of Lattice Spacings and Structures of Metals and Alloys**, Pergamon, Oxford, 1967 (1967).
- [30] H. D. Shashikala, S. V. Suryanarayana, S. V. Nagender Naidu, **Thermal expansion of stoichiometric ti3al**, Journal of Materials Science Letters 14 (11) (1995) 785–787 (Jan 1995). doi:[10.1007/BF00278128](https://doi.org/10.1007/BF00278128). URL <https://doi.org/10.1007/BF00278128>
- [31] K. Tanaka, M. Koiwa, **Single-crystal elastic constants of intermetallic compounds**, Intermetallics 4 (1996) S29–S39 (1996). doi:[10.1016/0966-9795\(96\)00014-3](https://doi.org/10.1016/0966-9795(96)00014-3). URL [http://dx.doi.org/10.1016/0966-9795\(96\)00014-3](http://dx.doi.org/10.1016/0966-9795(96)00014-3)
- [32] S. Banumathy, P. Ghosal, A. Singh, **On the structure of the ti3al phase in ti–al and ti–al–nb alloys**, Journal of Alloys and Compounds 394 (1) (2005) 181–185 (2005). doi:<https://doi.org/10.1016/j.jallcom.2004.10.029>. URL <http://www.sciencedirect.com/science/article/pii/S0925838804013751>
- [33] K. Tanaka, **Single-crystal elastic constants of  $\gamma$ -tial**, Philosophical Magazine Letters 73 (2) (1996) 71–78 (1996). arXiv:<https://doi.org/10.1080/095008396181019>, doi:[10.1080/095008396181019](https://doi.org/10.1080/095008396181019). URL <https://doi.org/10.1080/095008396181019>
- [34] Y. He, R. Schwarz, A. Migliori, S. Whang, **Elastic constants of single crystal  $\gamma$ -tial**, Journal of Materials Research 10 (5) (1995) 1187–1195 (1995). doi:[10.1557/JMR.1995.1187](https://doi.org/10.1557/JMR.1995.1187).
- [35] H. Hu, X. Wu, R. Wang, Z. Jia, W. Li, Q. Liu, **Structural stability, mechanical properties and stacking fault energies of tial3 alloyed with zn, cu, ag: First-principles study**, Journal of Alloys and Compounds 666 (2016) 185–196 (2016). doi:<https://doi.org/10.1016/j.jallcom.2016.01.106>.

- [36] M. Nakamura, K. Kimura, Elastic constants of tial3 and zral3 single crystals, *Journal of Materials Science* 26 (8) (1991) 2208–2214 (Jan 1991). doi:[10.1007/BF00549190](https://doi.org/10.1007/BF00549190). URL <https://doi.org/10.1007/BF00549190>
- [37] E. S. Fisher, C. J. Renken, Single-crystal elastic moduli and the hcp → bcc transformation in ti, zr, and hf, *Phys. Rev.* 135 (1964) A482–A494 (Jul 1964). doi:[10.1103/PhysRev.135.A482](https://doi.org/10.1103/PhysRev.135.A482). URL <https://link.aps.org/doi/10.1103/PhysRev.135.A482>
- [38] R. Watson, M. Weinert, *Phys. Rev. B* 58 (1998) 5981 (1998).
- [39] T. Novoselova, S. Malinov, W. Sha, A. Zhecheva, High-temperature synchrotron x-ray diffraction study of phases in a gamma tial alloy, *Materials Science and Engineering: A* 371 (1) (2004) 103 – 112 (2004). doi:<https://doi.org/10.1016/j.msea.2003.12.015>. URL <http://www.sciencedirect.com/science/article/pii/S0921509303014837>
- [40] A. V. Bakulin, A. M. Latyshev, S. E. Kulkova, Absorption and diffusion of oxygen in the ti3al alloy, *Journal of Experimental and Theoretical Physics* 125 (1) (2017) 138–147 (Jul 2017). doi:[10.1134/S1063776117070019](https://doi.org/10.1134/S1063776117070019). URL <https://doi.org/10.1134/S1063776117070019>
- [41] X. Zeng, R. Peng, Y. Yu, Z. Hu, Y. Wen, L. Song, Pressure effect on elastic constants and related properties of ti3al intermetallic compound: A first-principles study, *Materials* 11 (10) (2018). doi:[10.3390/ma11102015](https://doi.org/10.3390/ma11102015). URL <http://www.mdpi.com/1996-1944/11/10/2015>
- [42] F. Mouhat, F. m. c.-X. Coudert, Necessary and sufficient elastic stability conditions in various crystal systems, *Phys. Rev. B* 90 (2014) 224104 (Dec 2014). doi:[10.1103/PhysRevB.90.224104](https://doi.org/10.1103/PhysRevB.90.224104). URL <https://link.aps.org/doi/10.1103/PhysRevB.90.224104>
- [43] H. H. Wu, D. R. Trinkle, Direct diffusion through interpenetrating networks: Oxygen in titanium, *Phys. Rev. Lett.* 107 (2011) 045504 (Jul 2011). doi:[10.1103/PhysRevLett.107.045504](https://doi.org/10.1103/PhysRevLett.107.045504). URL <http://link.aps.org/doi/10.1103/PhysRevLett.107.045504>
- [44] L. Scotti, A. Mottura, Interstitial diffusion of o, n, and c in  $\alpha$ -ti from first-principles: Analytical model and kinetic monte carlo simulations, *The Journal of Chemical Physics* 144 (8) (2016) 084701 (2016). arXiv:<https://doi.org/10.1063/1.4942030>, doi:[10.1063/1.4942030](https://doi.org/10.1063/1.4942030). URL <https://doi.org/10.1063/1.4942030>
- [45] M. David, D. Connétable, Diffusion of interstitials in metallic systems, illustration of a complex study case: aluminum, *Journal of Physics: Condensed Matter* 29 (45) (2017) 455703 (2017). URL <http://stacks.iop.org/0953-8984/29/i=45/a=455703>
- [46] K. Hashi, K. Ishikawa, K. Suzuki, K. Aoki, Hydrogen absorption and desorption in the binary ti–al system, *Journal of Alloys and Compounds* 330-332 (2002) 547 – 550, proceedings of the International Symposium on Metal-Hydrogen Systems, Fundamentals and Applications (MH2000) (2002). doi:[https://doi.org/10.1016/S0925-8388\(01\)01660-7](https://doi.org/10.1016/S0925-8388(01)01660-7). URL <http://www.sciencedirect.com/science/article/pii/S0925838801016607>
- [47] H. Estupiñan, I. Uribe, P. Sundaram, Hydrogen permeation in gamma titanium aluminides, *Corrosion Science* 48 (12) (2006) 4216 – 4222 (2006). doi:<https://doi.org/10.1016/j.corsci.2006.04.010>. URL <http://www.sciencedirect.com/science/article/pii/S0010938X0600151X>
- [48] A. Sieverts, The absorption of gases by metals, *Zeitschrift für Metallkunde* 21 (1929) 37–46 (1929).
- [49] G. Henkelman, A. Arnaldsson, H. Jónsson, A fast and robust algorithm for bader decomposition of charge density, *Computational Materials Science* 36 (3) (2006) 354 – 360 (2006). doi:<https://doi.org/10.1016/j.commatsci.2005.04.010>. URL <http://www.sciencedirect.com/science/article/pii/S0927025605001849>
- [50] C. Varvenne, F. Bruneval, M.-C. Marinica, E. Clouet, Point defect modeling in materials: Coupling ab initio and elasticity approaches, *Phys. Rev. B* 88 (2013) 134102 (Oct 2013). doi:[10.1103/PhysRevB.88.134102](https://doi.org/10.1103/PhysRevB.88.134102). URL <https://link.aps.org/doi/10.1103/PhysRevB.88.134102>
- [51] D. Connétable, M. David, Diffusion of interstitial species (h and o atoms) in fcc systems (al, cu, co, ni and pd): Contribution of first and second order transition states, *Journal of Alloys and Compounds* 772 (2019) 280 – 287 (2019). doi:<https://doi.org/10.1016/j.jallcom.2018.09.042>. URL <http://www.sciencedirect.com/science/article/pii/S0925838818332717>
- [52] D. Matthieu, P. Aurélien, M. Daniel, C. Damien, First-principles study of the insertion and diffusion of interstitial atoms (h, c, n and o) in nickel, *Journal Alloys and Compounds* (submitted) (2019).
- [53] H. Eyring, The activated complex in chemical reactions, *The Journal of Chemical Physics* 3 (2) (1935) 107–115 (1935). arXiv:<https://doi.org/10.1063/1.1749604>, doi:[10.1063/1.1749604](https://doi.org/10.1063/1.1749604). URL <https://doi.org/10.1063/1.1749604>
- [54] K. Momma, F. Izumi, VESTA3 for three-dimensional visualization of crystal, volumetric and morphology data, *Journal of Applied Crystallography* 44 (6) (2011) 1272–1276 (Dec 2011). doi:[10.1107/S0021889811038970](https://doi.org/10.1107/S0021889811038970). URL <https://doi.org/10.1107/S0021889811038970>
- [55] S. Ishioka, M. Koiwa, Diffusion coefficient in crystals with multiple jump frequencies, *Philosophical Magazine A* 52 (2) (1985) 267–277 (1985). arXiv:<https://doi.org/10.1080/01418618508237623>, doi:[10.1080/01418618508237623](https://doi.org/10.1080/01418618508237623). URL <https://doi.org/10.1080/01418618508237623>